Journal of the Ceramic Society of Japan 123 [10] 983-988 2015 Paper

Assessment of carbon contamination in $MgAl_2O_4$ spinel during spark-plasma-sintering (SPS) processing

Koji MORITA,[*,†] Byung-Nam KIM,[*] Hidehiro YOSHIDA,[*] Keijiro HIRAGA[*,] and Yoshio SAKKA[*]**

[*]Advanced Ceramics Group, National Institute for Materials Science, 1–2–1 Sengen, Tsukuba, Ibaraki 305–0047, Japan
[**]Materials Science and Engineering, Kitami Institute of Technology, 165 Koencho, Kitami, Hokkaido 090–8507, Japan

Carbon contamination caused during spark-plasma-sintering (SPS) processing was investigated in the $MgAl_2O_4$ spinel by Raman spectroscopy. Although the carbon contamination became remarkable around the sample surfaces directly contacting the carbon paper, it sensitively changes with the SPS conditions, particularly for the heating rate. For the slow heating rate of 10°C/min, the carbon contamination can be detected around the surface regions rather than inside. For the high heating rate, however, a large amount of the carbon contamination was detected even inside in addition to the significant contamination around the surfaces even though the sintering temperature is the same and the processing time is shorter as compared to those of the slow heating rate. The present results suggest that the carbon contamination is not caused by diffusion processes, but caused by evaporation of the carbon phase from the carbon paper/dies, which were used in the SPS process. For the high heating rates, the carbon evaporation is enhanced due to the rapid heating and goes into the samples through open pore channels. The evaporated carbon is encapsulated into the closed pores during the heating process and remains along the grain junctions as glassy carbon.

Key-words : Spark-plasma-sintering, Carbon, Vacancy, Optical properties, Spinel

[Received May 8, 2015; Accepted July 28, 2015]

1. Introduction

The spark-plasma-sintering (SPS) technique is a powerful sintering tool and has widely been utilized to consolidate various types of materials; i.e., metallic alloys, ceramics and composites.[1)–4)] This is because the SPS technique can realize heating rates higher than 50°C/min, and hence, can complete the sintering process in a short time. It is reported, however, that the SPS processed oxides, such as Al_2O_3,[5)] ZrO_2[6),7)] and spinels,[8)–12)] exhibit a discoloration. Such a discoloration is known to be a typical phenomenon in the SPS processed oxides and appears to be more remarkable than the HIP/HP processed oxides.

The discoloration in the spinel can be explained by the combination of carbon contaminations and lattice defects (color centers), which are introduced in the spinel matrix, depending on the SPS conditions.[11),12)] Although the carbon contamination and defect formations can be reduced by decreasing the heating rate to some extent, they remain in the matrix even at the slow heating rate. The remaining lattice defects can be removed by post-annealing in air.[13)] For the carbon contamination, however, since the carbon contamination transforms into CO/CO_2 bubbles within the materials by the post-annealing in air due to the reaction with oxygen,[13)] it is very difficult to remove the carbon from the materials. In addition, although the lattice defects seem to mainly influence the transmission in the UV range, the carbon contamination is likely to affect the optical properties over a wide wavelength from the visible to infrared ranges.[12)] Therefore, the carbon contamination would cause serious problems in the SPS processed materials, especially for the oxide ceramics.

Although the discoloration has been explained by the carbon contamination, the experimental evidence is highly limited. In order to fully understand the contamination behavior during the SPS technique, the present study was therefore performed to measure the carbon distribution under several SPS conditions using a spinel ($MgAl_2O_4$) as the reference material.

2. Experimental procedures

Commercially available high purity magnesium aluminate spinel ($MgAl_2O_4$) powder (TSP-15, Taimei Chemical Co., Ltd., Tokyo, Japan) was used in this study. The stoichiometric spinel powder has a commercial purity of >99.97% and a particle size of 100–300 nm. The starting powder was consolidated using a spark-plasma-sintering (SPS) machine (SPS-1050, Fuji Electronic Industrial Co., Ltd., Saitama, Japan) under vacuum higher than 1 Pa. The details were described elsewhere.[11)–16)]

Briefly, the starting powder was placed in a graphite die with a 30 mm inner diameter as shown in **Fig. 1**. The powder was isolated from the graphite die/punch by carbon papers, which were placed between the powder and the graphite die/punch. The graphite die was covered with thermal insulator carbon felt to suppress heat losses from the die surfaces. The SPS processing was carried out at a uniaxial pressure of 80 MPa, heating rates of $\alpha = 10$ and 100°C/min, a temperature of $T = 1300$°C and a soaking time of $t_s = 20$ min. The SPS condition was determined based on the following reasons. The applied pressure was selected based on the maximum available stress of the carbon die used in this study. The heating rate of $\alpha = 100$°C/min has been regarded as the primary advantage of the SPS technique and has been widely used in the SPS processing. For the present spinel, however, the best transmission can be attained at the combination of $\alpha = 10$°C/min, $T = 1300$°C and $t_s = 20$ min. Since the heating rate strongly affects the carbon contamination,[11),12)] the effect of α on the carbon distribution was mainly examined under the constant load, T and t_s conditions. The SPS temperature was controlled by measuring the surface temperature of the graphite

† Corresponding author: K. Morita; E-mail: MORITA.Koji@nims.go.jp

DOI http://dx.doi.org/10.2109/jcersj2.123.983

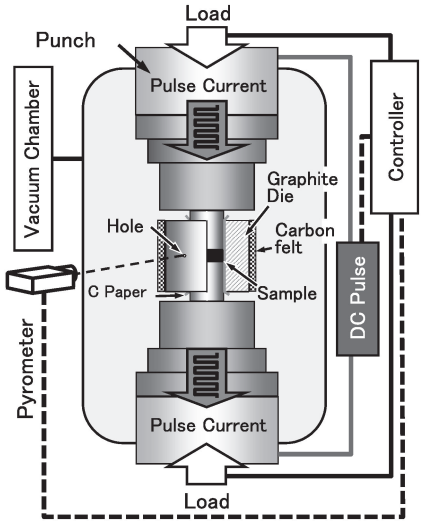

Fig. 1. Schematic configuration of the experimental setup of the SPS processing.[1)–4)]

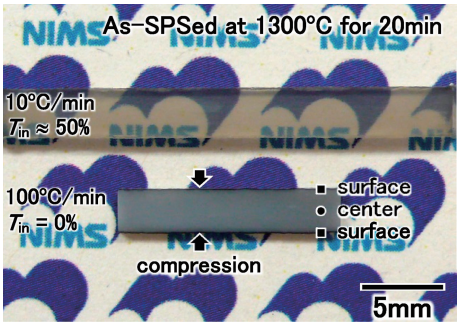

Fig. 2. Optical micrograph of the cross sectional view of the spinel disks SPSed at $T = 1300$°C for $t_s = 20$ min. The SPS processing was carried out at slow and high heating rates of $\alpha = 10$°C/min (upper) and 100°C/min (lower), respectively.

die using an optical pyrometer through a small window made in the carbon felt. By this procedure, we fabricated a circular disk with a 30 mm diameter and about 3 mm thickness.

The optical and phase characterizations were carried out at the cross section of the SPSed circular disks. The plates with a thickness of about 1.5 mm were cut from near the center of the circular disks. For the measurement of the in-line transmission T_{in}, both surfaces of the plates were carefully mirror-polished with diamond pastes and finished with a colloidal silica suspension. During the polishing procedures, the thickness of the plate was reduced to about 1 mm. The T_{in} measurement was conducted using a double-beam spectrophotometer (SolidSpec-3700DUV, Shimazu Co. Ltd., Japan) equipped with an integrating sphere. The carbon contamination was measured by a Raman spectrometer (Horiba-Jobin-Yvon T64000, Horiba Co. Ltd., Japan) using tahe Ar laser exciting wavelength of $\lambda_{exc} = 514.5$ nm.

3. Results and discussion

3.1 Spinel SPSed at 1300°C and heating rates of $\alpha = 10$°C/min and 100°C/min

Figure 2 shows the cross sectional view of the spinel plates, which were sliced from the circular disks SPSed at the slow and high heating rates of $\alpha = 10$°C/min (upper) and 100°C/min (lower). The SPS pressure was applied in the longitudinal direction as indicated by the arrows, and hence, the upper/bottom planes in the photo are the surfaces directly contacting the carbon paper. In this study, however, the sintering direction was not verified, hence, the upper/bottom does not necessarily correspond to the direction of the setup of the SPS process.

For the slow heating rate, the spinel shows optical transmission and the text is clearly visible through the spinel plate, as reported in our previous studies.[11),14),15)] For the high heating rate, however, the spinel is opaque even for the same sintering conditions as the slow heating rate; i.e., a sintering pressure of 80 MPa, $T = 1300$°C and $t_s = 20$ min. For the as-SPSed spinel, the in-line transmission evaluated at a wavelength of $\lambda = 550$ nm, $T_{in,550}$, reaches about 50% for the former, but is 0% for the latter. Although the spinel SPSed at the slow heating rate shows the visible light transmission of $T_{in,550} \approx 50\%$, the attained value is lower than that of the HIPed spinel; it shows a higher transmission similar to the theoretical value ($T_{th} \approx 87\%$).[17)–19)] This difference is related to discoloration; the HIPed spinel does not show any discoloration, but the present SPSed spinels unfortunately reveal a discoloration irrespective of the heating rate, as shown in Fig. 2.

3.2 Raman measurement

It is confirmed in our recent studies that the discoloration of the spinel is influenced by two factors, which are formed during the SPS processing.[11),12)] One factor can be ascribed to carbon contamination; the other is lattice/point defects formation. Although the Raman spectroscopic technique is an effective method to estimate the carbon phases, it is known to be influenced by several parameters, such as λ_{exc},[20),21)] the operating power OP, the recording time t_r, etc. Since the carbon contamination in the SPSed spinel is extremely small,[11)–13)] the parameters should be optimized.

Figures 3(a) and 3(b) show an example of the Raman spectra, which are measured by changing the parameters, such as OP and t_r, for optimization. This measurement is carried out at the same position in the center region of the spinel plate SPSed at $\alpha = 10$°C/min. It is apparent that although the Raman peaks relating to the D- and G-bands are very weak for the lower operating power OP and the shorter recording time t_r, they become clear with the increasing OP and t_r. The peak intensities I obtained at several OP and t_r are plotted in Figs. 3(c) and 3(d), respectively, after normalizing with the reference data I_{ref} obtained at OP = 100 mW and $t_r = 40$ s. The normalized peak intensities I/I_{ref} of the D- and G-bands tend to linearly decrease with OP and t_r. Hence, it can be assumed that for the measurement at OP = 50 mW and $t_r = 20$ s, the I-values would be reduced to about 25% of the reference intensity I_{ref}.

The increase in the parameters, OP and t_r, can also increase the detectable power. However, the OP = 100 mW is the upper limit of the machine utilized in this study and an increase in t_r merely consumes time. Thus, in the present study, the Raman measurement was determined to be measured at OP = 100 mW, $t_r = 40$ s and an accumulation number of 10 times.

3.3 Raman spectrum of starting spinel powder

The Raman spectrum of the starting spinel powder is shown in the bottom of **Figs. 4** through **6**. As shown in Fig. 4, the Raman spectrum shows five major peaks around 311, 410, 672, 727 and 770 cm^{-1}. These can be assigned as the typical vibration modes of the $MgAl_2O_4$ spinel; $E_g = 410\,cm^{-1}$, $A_{1g} = 770\,cm^{-1}$, $T_{2g} = 311$, $672\,cm^{-1}$ [22)–24)] and the breathing mode of BM = 727 cm^{-1}.[24)] In addition to the typical vibration modes of the spinel,

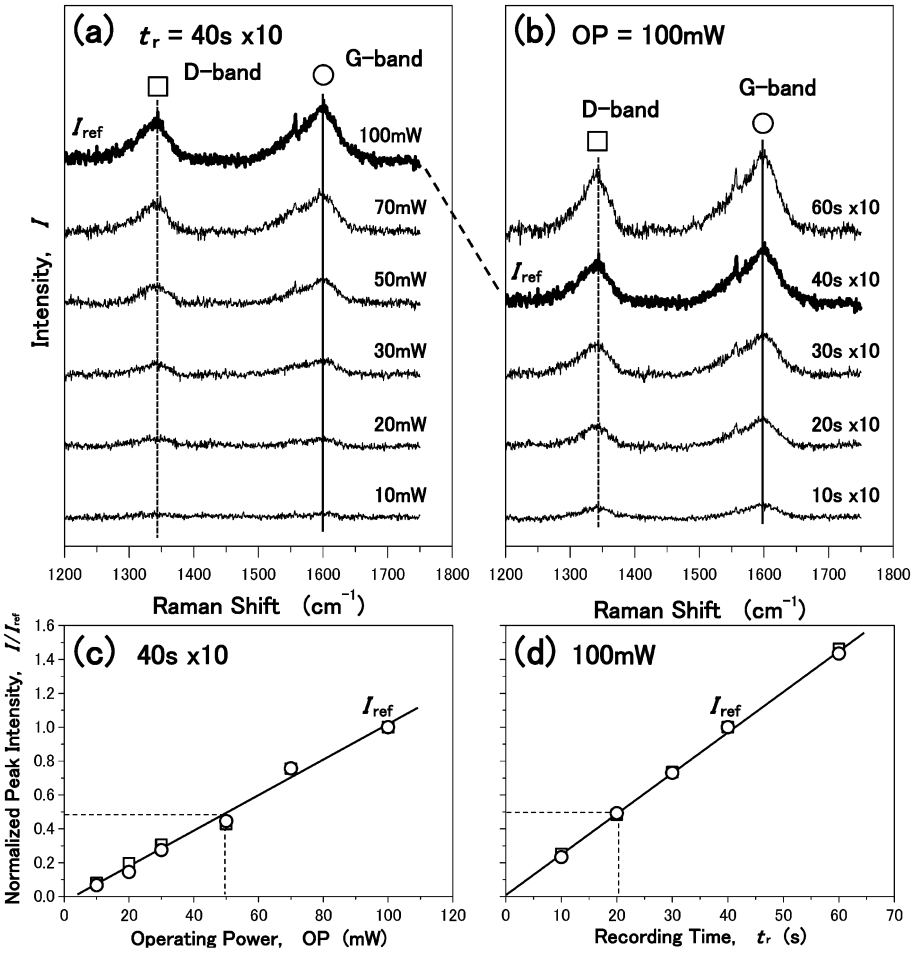

Fig. 3. Raman spectra from 1200 to 1800 cm^{-1} taken at the center region of the spinel plate SPSed at $T = 1300$°C for $t_s = 20$ min and at $\alpha = 10$°C/min. (a) OP dependence at $t_r = 40$ s and an accumulation number of 10, and (b) t_r dependence at an accumulation number of 10 and OP = 100 mW. (c) OP- and (d) t_r-dependent peak intensities of the D- and G-bands are plotted after normalized by the reference data I_{ref} [thick line in (a) and (b)] obtained at OP = 100 mW and $t_r = 40$ s × 10.

the spectrum exhibits four additional minor peaks at around 157, 233, 560 and 1064 cm^{-1}. The minor peaks around 157 and 1064 cm^{-1} (solid arrows) can be assigned to the external vibration of the carbonate CO_3^{2-} group[25] and the ν_1 symmetric C–O stretching mode of CO_3,[2–26] respectively. Other minor peaks around 233 and 560 cm^{-1} can be ascribed to the vibration of chlorine Cl*; the A_{1g} breathing mode of the Mg–Cl octahedral in $MgCl_2$ at 233 cm^{-1} [27] (broken line) and the Cl_2 signal at 560 cm^{-1} [28] (open arrow). This indicates that the starting powder contains carbonate CO_3^{2-} and chlorine Cl_2 as minor impurities.[11]

3.4 Carbon contaminant distribution of SPSed spinel

The Raman spectra taken from the spinel plates are shown in Figs. 4 through 6. The spectra are measured at several positions of the cross section between the upper/bottom surfaces (Fig. 2).

Figure 4 shows an example of the Raman spectra, which are taken from the surface and the center of the spinel plate SPSed at $\alpha = 10$°C/min. In the wavelength range of 100–1150 cm^{-1}, the spectra of the as-SPSed spinels exhibited almost the same characteristic, irrespective of the position and the heating rate, α, as typically shown in Fig. 4, and no apparent difference can be found in the spectra. This characteristic, however, is slightly different from that of the starting powder. The spectra also show five active vibration modes typical for the $MgAl_2O_4$ spinel; E_g = 410 cm^{-1}, A_{1g} = 770 cm^{-1}, T_{2g} = 311 and 672 cm^{-1},[21)–23)] and BM = 727 cm^{-1}.[23] In the SPSed spinels, although the vibration mode A_{1g} of $MgCl_2$ remains at 233 cm^{-1} (broken-line) as well as the powder, the vibration modes of the trace Cl_2 and CO_3^{2-} at 157, 560 and 1064 cm^{-1} disappear.

Figure 5(a) shows the Raman spectra in the range of 1200–1750 cm^{-1} measured at several positions of the spinel SPSed at $\alpha = 10$°C/min. It is noteworthy that the Raman spectra of this SPSed spinel exhibit two broad peaks at around 1350 and 1600 cm^{-1}. Since the two peaks are not detected in the powder (bottom), they might be formed during the SPS processing. For comparison, the Raman spectra taken from the carbon paper and graphite die used in this study are also shown in the upper part of Fig. 5(a). The two new peaks almost coincide with those of the paper/die, suggesting that these peaks can be ascribed to the D- and G-bands arising from carbon phases.[11),12)] The D-band is related to the disordered structure in the sp^2-network of the carbon phases. Since the spectra clearly show the disorder-induced D-band and these peaks are broad, they may be related to the disordered sp^2 carbon phases, such as the glassy carbon and/or graphite oxide (GO) phases.[29),30)]

* According to the private communication of Taimei Chemical Co., the spinel powder seems to contain a small amount of chlorine as a contaminate.[10]

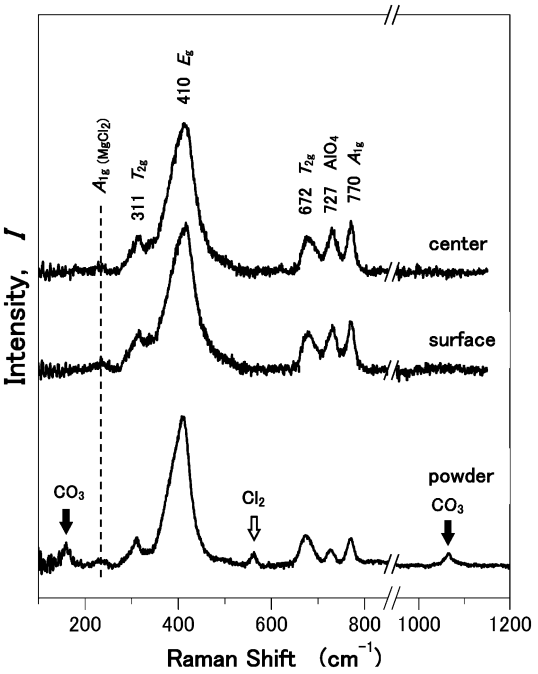

Fig. 4. Typical Raman spectra in the range of 100–1200 cm^{-1} of the starting spinel powder (bottom) and the spinel plate. The Raman spectra of the spinel plate, which was SPSed at $T = 1300$°C for $t_s = 20$ min and at $\alpha = 10$°C/min, were taken from the sample surface and the center regions for comparison.

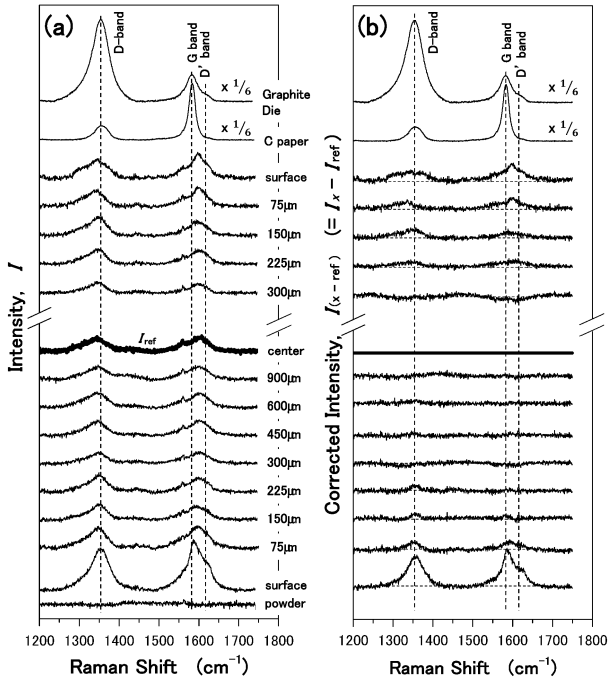

Fig. 5. (a) Typical Raman spectra in the range of 1200–1800 cm^{-1} of the starting spinel powder (bottom) and the spinel plate SPSed at $T = 1300$°C for $t_s = 20$ min and at $\alpha = 10$°C/min. The spectra of the spinel plate are taken from several positions of the cross section. The number written in each spectrum is the position x distance from the upper/bottom surfaces. (b) Corrected Raman spectra $I_{(x-ref)}$ of (a) after subtracting the intensity I_{ref} of the center as a reference data. For comparison, the Raman spectra of the graphite die and carbon paper are also shown in the upper part of (a) and (b) after reducing the spectrum intensities I to 1/6.

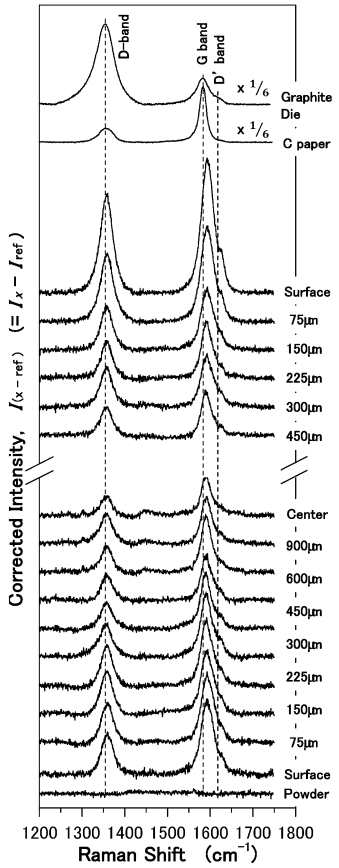

Fig. 6. Typical Raman spectra in the range of 1200–1800 cm^{-1} of the starting spinel powder (bottom) and the spinel plate SPSed at $T = 1300$°C for $t_s = 20$ min and at $\alpha = 100$°C/min. The spectra were re-plotted after subtracting the intensity I_{ref} of the reference spectrum, which was taken from the center of the spinel plate SPSed at 1300°C for 20 min and at $\alpha = 10$°C/min.

In addition, it was also found from Fig. 5(a) that the two peaks related to the D/G-bands are not constant, but change with the position x, which is the distance from the upper/bottom surfaces of the spinel plate. The peak intensities I_x are apparently higher near both the upper/bottom surfaces than at around the inside region between $x > 300$ μm and the center. As noted in previous studies,[11),12)] during the SPS processing, the trace CO_3^{2-} pre-existing in the starting powder transforms into the carbon phases and remains into the SPSed spinel as glassy carbon. Since the amount of the pre-existing CO_3^{2-} might be constant for each batch/position, the amount of the carbon phases transformed from CO_3^{2-} should also be constant. Hence, the higher I_x-value at the surfaces cannot be explained only by the pre-existing CO_3^{2-}. The position-dependent peak intensity I_x in Fig. 5(a) suggests that the carbon contamination is not caused only from the pre-existing trace CO_3^{2-}, but additionally from the outside during the SPS processing.

The carbon peaks taken from the center region are not affected from the outside, and hence, can be ascribed to the carbon phases transformed only from the pre-existing trace CO_3^{2-}. By using the spectrum intensity of the center I_{ref} as a reference, the carbon contamination additionally caused during the SPS processing can be estimated by subtracting I_{ref} from I_x, as shown in Fig. 5(b). Figure 5(b) shows that for the inside region of $x > 300$ μm, the corrected intensities $I_{(x-ref)}$ ($= I_x - I_{ref}$) become almost flat, suggesting that the carbon contamination is constant and is mainly

caused by the pre-existing CO_3^{2-} impurity. For the surface region of $x < 225\,\mu m$, however, the $I_{(x-ref)}$-values still show the D/G-bands and tend to increase while approaching the surfaces. This indicates that the carbon contamination around the surface region ($x < 225\,\mu m$) occurs additionally from the paper/die.

The characteristic of the D/G-bands also changes with the heating rate α. Figure 6 shows the Raman spectra of the spinel SPSed at $\alpha = 100°C/min$. In order to eliminate the influence of the pre-existing CO_3^{2-} impurity, the spectra were plotted after subtracting the reference intensity I_{ref} of the spinel SPSed at $\alpha = 10°C/min$. Thus, the corrected spectra $I_{(x-ref)}$ in Fig. 6 can be ascribed only to the carbon contamination additionally coming from the outside during the SPS processing.

In contrast to that of $\alpha = 10°C/min$, the corrected intensities $I_{(x-ref)}$ of $\alpha = 100°C/min$ show the D/G-bands for the entire region from the surfaces to the center. This indicates that for $\alpha = 100°C/min$, the carbon contamination occurs over the entire region, at least for a 3 mm in thickness. In addition, the spectrum of $I_{(x-ref)}$ is much sharper and higher for $\alpha = 100°C/min$ than for $\alpha = 10°C/min$. The peak intensity ratio of the disorder-induced D-band and the G-band, (I_D/I_G) has generally been used to quantify the relative amount of the disordered structure in the carbon phases. For $\alpha = 10°C/min$, the carbon phases can be ascribed to the glassy carbon and/or GO phases due to the higher I_D/I_G ratio of ≈ 1 and their broad peaks. For $\alpha = 100°C/min$, on the other hand, the I_D/I_G ratio is a relatively lower value of ≈ 0.5–0.7, suggesting that they are no longer the disordered carbon phases, but are likely to have further organized structures. This indicates that increasing the heating rate during the SPS process enhances the carbon contamination from the paper/die. The trend in the lower I_D/I_G ratio resembles that of the carbon paper rather than that of the die. Based on the I_D/I_G ratio, although the carbon contamination may occur from both the paper/die, it is more likely to significantly originate from the carbon paper.

The additional carbon contamination cannot be explained by solid diffusion processes. This is because if the contamination was caused by solid diffusion processes, it should increase at $\alpha = 10°C/min$ due to its longer processing time. Furthermore, the temperature and dwelling time also do not enhance the contamination.[12] Since the direct hard evidence to determine the contamination mechanism has not yet been obtained, a comprehensive understanding of the mechanism is difficult in the present study. Nevertheless, in order to explain the carbon contamination the occurred from the sample surface to the deep inside areas, contamination mechanisms related to gaseous carbon is more likely to be appropriate. It is reasonable to explain, therefore, that the additional carbon contamination would be mainly caused by evaporation of the carbon phase during the heating process.[11),12)]

For the high heating rate, which is a primary advantage of the SPS technique,[1)–4)] evaporation of the carbon phase from the paper/die is considered to be enhanced probably due to the rapid heating and/or higher applied pulse current. The evaporated carbon would go deep inside the sample through the open pore channels and encapsulate into the closed pores during the heating process. The encapsulated carbon would remain in the matrix as glassy carbon and/or GO phases. With an increase in the heating rate, the amount of the carbon contamination, namely, the degree of stacking orders, increases and this results in the organized carbon phases as shown in Fig. 6. Although the carbon distribution becomes remarkable on both surfaces irrespective of the heating rate, the trend in the distribution is slightly different between both surfaces. This suggests that the direction of the pulse current in the SPS processing may affect the slight difference in the contamination. In this study, however, the upper/bottom surfaces in the SPS setup were not verified, and hence, the directional dependent contamination cannot be discussed.

The Raman spectroscopic technique can clearly show the SPS condition dependence of the carbon contamination behavior in the spinel. Especially, the reported data successfully indicated that the heating rate must be one of the critical factors that affects the carbon contamination. The Raman technique, however, is highly sensitive only to the order/disordered carbon phases having the sp^2/sp^3 bonding state and cannot detect the individual carbon atoms. Hence, if the carbon atoms also exist along the grain boundaries or within the grains as impurities, other techniques should be utilized for further discussion. However, if individual carbon atoms exist within the grains, they create absorption bands in the transparent spectrum due to the formation of point defects.[31)] This is not the case in the present study because the spectrum monotonously changed with the wavelength of the incident light.[14)–16)] Accordingly, it can be concluded that the carbon phases contaminated from the pre-existing CO_3^{2-} and from the paper/die exist along the grain boundary and the multiple grain junctions. The carbon contaminations caused from the paper/die also occurred in other oxide ceramics, such as Al_2O_3 and ZrO_2.[13)] In order to reduce the contamination, the heating rate should be reduced as much as possible though the high heating rate is a primary advantage of the SPS technique, otherwise other die systems may need to be considered instead of the carbon.

4. Summary

Discoloration of the SPSed $MgAl_2O_4$ spinel was examined by Raman spectroscopic techniques. The results obtained in this study are as follows:

1) Depending on the SPS condition, the carbon contamination occurs in the spinel from the carbon paper/dies used in the sintering process.
2) For the slow heating rate of $\alpha = 10°C/min$, the contamination occurs only around the surface regions of $x < 300\,\mu m$, but not into the inside region, except for the carbon contamination transformed from the CO_3^{2-} impurity pre-existing in the starting powder.
3) For the high heating rate of $\alpha = 100°C/min$, although the carbon contamination occurs over almost the entire region of the spinel plate with a 3 mm thickness, the amount of the contamination is significant around the surfaces. With the increasing heating rate, the carbon contamination tends to be organized.
4) The carbon contamination is caused by evaporation of the carbon phase from the carbon paper/dies. For the high heating rates, the carbon evaporation is enhanced due to the rapid heating and goes into the samples through the open pore channels. The evaporated carbon is encapsulated in the closed pores during the heating process and remains along the grain boundary and the multiple grain junctions.

Acknowledgement This study was financially supported by the Amada Foundation (AF-2014020) and the Grant-in-Aid for Scientific Research [(C)25420700 and (C)15K06515] from the Ministry of Education, Culture, Sports, Science and Technology (MEXT), Japan.

References

1) M. Omori, *Mater. Sci. Eng., A*, **287**, 183–188 (2000).
2) Z. A. Munir, U. Anselmi-Tamburini and M. Ohyanagi, *J. Mater. Sci.*, **41**, 763–777 (2006).

3) R. Orrù, R. Licheri, A. M. Locci, A. Cincotti and G. Cao, *Mater. Sci. Eng., R*, 63, 127–287 (2009).
4) S. Grasso, Y. Sakka and G. Maizza, *Sci. Technol. Adv. Mater.*, 10, 053001 (2009).
5) D. T. Jiang, D. M. Hulbert, U. Anselmi-Tamburini, T. Ng, D. Land and A. K. Mukherjee, *J. Am. Ceram. Soc.*, 91, 151–154 (2008).
6) U. Anselmi-Tamburini, J. N. Woolman and Z. A. Muni, *Adv. Funct. Mater.*, 17, 3267–3273 (2007).
7) H. Zhang, B.-N. Kim, K. Morita, H. Yoshida, K. Hiraga and Y. Sakka, *Sci. Technol. Adv. Mater.*, 12, 055003 (2011).
8) S. Meir, S. Kalabukhov, N. Froumin, M. P. Dariel and N. Frage, *J. Am. Ceram. Soc.*, 92, 358–364 (2009).
9) G. Bernard-Granger, N. Benameur, C. Guizard and M. Nygren, *Scr. Mater.*, 60, 164–167 (2009).
10) B. N. Kim, K. Morita, J. H. Lim, K. Hiraga and H. Yoshida, *J. Am. Ceram. Soc.*, 93, 2158–2160 (2010).
11) K. Morita, B.-N. Kim, H. Yoshida, K. Hiraga and Y. Sakka, *Acta Mater.*, 84, 9–19 (2015).
12) K. Morita, B.-N. Kim, H. Yoshida, K. Higara and Y. Sakka, *J. Am. Ceram. Soc.*, 98, 378–385 (2015).
13) K. Morita, B.-N. Kim, H. Yoshida, K. Higara and Y. Sakka, to be submitted to *J. Euro. Ceram. Soc.*, (2015).
14) K. Morita, B.-N. Kim, K. Hiraga and H. Yoshida, *Scr. Mater.*, 58, 1114–1117 (2008).
15) K. Morita, B.-N. Kim, K. Hiraga and H. Yoshida, *J. Am. Ceram. Soc.*, 92, 1208–1216 (2009).
16) K. Morita, B.-N. Kim, H. Yoshida and K. Hiraga, *J. Mater. Res.*, 24, 2863–2872 (2009).
17) A. Krell, J. Klimke and T. Hutzler, *Opt. Mater.*, 31, 1144–1150 (2009).
18) A. Krell, J. Klimke and T. Hutzler, *J. Eur. Ceram. Soc.*, 29, 275–281 (2009).
19) A. Krell, T. Hutzler, J. Klimke and A. Potthoff, *J. Am. Ceram. Soc.*, 93, 2656–2666 (2010).
20) Y. Wang, D. C. Alsmeyer and R. L. McCreery, *Chem. Mater.*, 2, 557–563 (1990).
21) Z. H. Ni, H. M. Fan, Y. P. Feng, Z. X. Shen, B. J. Yang and Y. H. Wu, *J. Chem. Phys.*, 124, 204703 (2006).
22) I. Ganesh, *Int. Mater. Rev.*, 58, 63–112 (2013).
23) M. P. O'Horo, A. L. Frisillo and W. B. White, *J. Phys. Chem. Solids.*, 34, 23–28 (1973).
24) M. Lazzeri and P. Thibaudeau, *Phys. Rev. B*, 74, 140301 (2006).
25) S. Gunasekaran, G. Anbalagan and S. Randi, *J. Raman Spectrosc.*, 37, 892–899 (2006).
26) R. L. Frost, J. Čejka, G. A. Ayoko and M. J. Dickfos, *J. Raman Spectrosc.*, 39, 374–379 (2008).
27) C. R. Tewell, F. Malizia, J. W. Ager III and G. A. Somorjai, *J. Phys. Chem. B*, 106, 2946–2949 (2002).
28) W. F. Howard, Jr. and L. Andrew, *Inorg. Chem.*, 14, 767–771 (1975).
29) M. Osada and M. Kakihana, *TANSO*, 228, 174–184 (2007) [in Japanese].
30) K. N. Kudin, B. Ozbas, H. C. Schniepp, R. K. Prud'homme, I. A. Aksay and R. Car, *Nano Lett.*, 8, 36–41 (2008).
31) A. Goldstein, A. Shames, A. J. Stevenson, Z. Cohen and M. Vulfson, *J. Am. Ceram. Soc.*, 96, 3523–3529 (2013).